




# Synergistic Effect of Graphene Nanoplatelets and Multiwall Carbon Nanotubes Incorporated in PLA Matrix: Nanoindentation of Composites with Improved Mechanical Properties

Todor Batakliiev , Vladimir Georgiev, Verislav Angelov, Evgeni Ivanov, Cristiane Kaluggian, Pablo A.R. Muñoz, Guilhermino J.M. Fechine, Ricardo J.E. Andrade, and Rumiana Kotsilkova

Submitted: 29 September 2020 / Revised: 4 March 2021 / Accepted: 12 March 2021

The synergistic effect of two carbon nanofillers on the mechanical properties of PLA-based nanocomposites was investigated in the present work. Polylactic acid is relatively brittle semi-crystalline polymer which was selected for composite matrix because of its biodegradable properties. It was reinforced with graphene nanoplatelets and multiwall carbon nanotubes by means of melt mixing preparation method. Nanohardness and Young's modulus of smooth nanocomposite samples received by 3D printing were defined by nanoindentation experiments using Berkovich-type pyramidal nanoindenter. It was found that the compounds, incorporated with both graphene and carbon nanotubes in the polymer structure, exhibit better mechanical performance compared to the nanocomposites loaded with a single carbon nanofiller. Different techniques of sample preparation were applied in order to see the influence of preliminary processing on the nanomechanical properties of composite specimens. X-ray diffraction and Raman spectroscopy were used to study the structural features of the pristine carbon nanomaterials.

**Keywords** carbon nanofillers, composites, nanoindentation, nanoscratch, polylactic acid, structure analysis, synergism

## 1. Introduction

Depth-sensing indentation (DSI) or also denoted as nanoindentation technique represents nowadays one of the main techniques for mechanical characterization of wide range of materials as polymer-based nanocomposites, coated materials, titanium alloys, metallic glasses, single-crystals or heterogeneous structural materials (Ref 1-6). The method follows the penetration of an indenter into the material surface during the application and release of constant force. Considering composites loaded with graphene or other carbon material the

nanoindentation appears to be a really valuable tool for the evaluation of the Young's modulus and hardness enhancements upon incorporation of the filler (Ref 7). At the present time, the most advanced nanoindentation instruments can perform indentations with contact depths of only a few tens of nanometers, most of them also offering the possibility of approaching an upper limit in the micron regime (Ref 8).

Polymer matrix composites suggest high specific strength and elasticity (Ref 9). Moreover, they are relatively more susceptible for precise uniform manufacturing of complex preshaped products (Ref 10). Recently, the polylactic acid-based composites have been widely studied and used because of their mechanical and biodegradable properties (Ref 11). Considerably features enhancement can be obtained by reinforcing the polymer with relatively small amounts of nanomaterials, which are nanosized at least in one dimension (Ref 12). It has been found that the graphene sheets consist of wrinkled structures and in between the wrinkles there are sections having surface roughness of  $\sim 4\text{-}5 \text{ \AA}$ . This surface roughness could present a preferential nucleation site for crystalline phases when graphene is dispersed in a polymer matrix (Ref 13). Polyvinyl alcohol (PVA) and poly(methyl methacrylate) (PMMA)-matrix composites reinforced by functionalized few-layer graphene (FG) have been evaluated using the nanoindentation technique. The experiments were carried out at loads of 5 and 8 mN depending on composite type. In spite of the reported increase of hardness and elasticity with boosting graphene content, the obtained values are relatively low. For the PVA composites, the elastic modulus is in the range 0.657-0.885 GPa and the resulting hardness is between 38.0 and 55.7 MPa. It should be mentioned that the displacement during the nanoindentation is reaching 2.75  $\mu\text{m}$  taking into account the negligible applied force (Ref 14). In another article (Ref 15), a maximum load of 1 mN has been used during nanoindentation of polyvinyl alcohol

**Todor Batakliiev, Vladimir Georgiev, and Evgeni Ivanov**, Open Laboratory on Experimental Micro and Nano Mechanics (OLEM), Institute of Mechanics, Bulgarian Academy of Sciences, Acad. G. Bonchev Str. Block 4, 1113 Sofia, Bulgaria; and Research and Development of Nanomaterials and Nanotechnologies (NanoTech Lab Ltd.), Acad. G. Bonchev Str. Block 4, 1113 Sofia, Bulgaria; **Verislav Angelov and Rumiana Kotsilkova**, Open Laboratory on Experimental Micro and Nano Mechanics (OLEM), Institute of Mechanics, Bulgarian Academy of Sciences, Acad. G. Bonchev Str. Block 4, 1113 Sofia, Bulgaria; and **Cristiane Kaluggian, Pablo A.R. Muñoz, Guilhermino J.M. Fechine, and Ricardo J.E. Andrade**, MackGraphe, Mackenzie Institute for Research in Graphene and Nanotechnologies, Mackenzie Presbyterian University, Rua da Consolação, São Paulo, SP 89601302-907, Brazil. Contact e-mail: todorbat@gmail.com.

matrix incorporated with binary combinations of nanodiamond, few-layer graphene, and single-walled nanotubes. The mechanical properties of the resulting composites, evaluated by the nanoindentation technique, have shown extraordinary synergy regarding the composites with single-walled nanocarbon as a part of bifiller reinforcement. The authors have attributed this significant increase to high aspect ratio of the nanotubes as well as to the preventing role of nanodiamond particles against SWNTs clustering due to Van der Waals interactions. They also referred the acid functionalization of SWNTs contributing to better bonding with the polymer because of the presence of surface carboxyl and hydroxyl groups.

The effect of graphene nanoplatelets (GNPs) on mechanical properties of epoxy-based vinyl ester polymer nanocomposites has been investigated using nanoindentation and nanoscratch methods (Ref 16). The GNPs at different low weight fractions up to 0.5% were dispersed in the polymer matrix. A standard Berkovich indenter was used for indentation at three different normal loads, i.e., 400, 600 and 800  $\mu\text{N}$ . The authors reported around 30% improvement of both elastic modulus and hardness with the addition of graphene nanoplatelets and up to 400 nm surface displacement at load of 800  $\mu\text{N}$ . Hwang et al. have shown the positive effect of raising the content of graphene flakes, expressed by better mechanical properties of PMMA/graphene composite spin-coated on Si substrate for nanoindentation study (Ref 17). Applying force of 100 mN at 16 positions, they received a significant increase in hardness and elasticity for 1.0 wt.% graphene loading in the PMMA-based composite. The combination of high aspect ratio of CNTs and larger surface area of GNPs was described to have an important contribution to the synergistic effect of nanofiller hybrids concerning the mechanical properties of epoxy composites (Ref 18).

The current literature on instrumented indentation provides apparently conflicting information about the synergistic effect of more than one carbon nanofiller on the nanomechanical performances of polymer composites. Moreover, there is a lack of research papers dedicated to mechanical characteristics assignment of PLA-based composites by using nanoindentation method. It might be a consequence of the tough process of elaborating test samples possessing enough surface flatness. In the present study, the synergistic effect of graphene nanoplatelets (GNPs) and multiwall carbon nanotubes (MWCNTs) on the mechanical properties enhancement of biodegradable polymer composites has been investigated by employing of precise nanoindentation and nanoscratch techniques.

## 2. Experimental

### 2.1 Materials

Ingeo™ Biopolymer PLA-3D850 with MFR 7-9 g/10 min (210°C, 2.16 kg) was purchased from Nature Works (USA). TNIGNPs—Industrial Graphene Nanoplatelets—average thickness < 30 nm and mean size of  $\sim$  5-7  $\mu\text{m}$ ; purity 90% and MWCNTs—OH-functionalized Multiwall Carbon Nanotubes—outer diameter  $\sim$  10-30 nm and length of  $\sim$  10-30  $\mu\text{m}$ ; SSA = 110  $\text{m}^2/\text{g}$ ; EC >100 S/cm; purity 95% were supplied from TimesNano (China). Black Magic in shape of filament was bought by Graphene Laboratories Inc. (NY, USA).

### 2.2 Preparation of Nanocomposites and Design of Test Samples

Monofiller (GNP/PLA and MWCNT/PLA) and bifiller (GNP/MWCNT/PLA) nanocomposites have been made by means of melt extrusion technique. The compounds were prepared through direct mixing of PLA and carbon nanofiller in the barrel of corotational twin screw extruder, COLLIN Teach-Line ZK25T, at screw speed of 40 rpm and temperature of 170-180°C. Composite plates with geometry 60  $\times$  12  $\times$  2.4 mm, printing density of 100% and possessing very low surface roughness were prepared by 3D printing using filament with diameter of 1.75 mm and applying FDM technique and layer-to-layer deposition. The set of samples was made with German RepRap X-400 Pro 3D printer having two printing heads and equipped with Simplify3D slicer.

The specimens were laid down in flat build orientation under nozzle temperature of 210°C, layer thickness of 0.25 mm and printing speed of 2600 mm/min. All samples were held in a vacuum package or a desiccator in order to protect them from air humidity. The composites analyzed by nanoindentation are listed in Table 1. Nanomechanical experiments were made on composite hot pressed films (20 mm diameter area) of 1 mm thickness, 3D-printed specimens (60  $\times$  12  $\times$  2.4 mm) and extruded filaments in order to see the influence of the specific sample layout. Prior to nanoindentation, the filaments were cut on microtome Leica RM2245 using diamond knife. This procedure was needful to get flat enough sample surface for reliable testing.

### 2.3 Characterization Methods

The pure carbon nanofillers were characterized by physical methods as Raman spectroscopy and XRD. Single spectra were taken on confocal microscope Raman spectrometer Witec Alpha 300R, using a 50  $\times$  excitation green argon ion laser with 600 g/mm grating. The power radiation was 3 mW at 532 nm wavelength edge laser physics and 0.5 s integration time. A laser beam with diameter of approximately 2.5  $\mu\text{m}$  was focused onto the surface of the carbon nanopowder. The crystalline structure of GNPs and MWCNTs was studied by x-ray diffraction performed on a Rigaku diffractometer, model Miniflex II, with a copper monochromator,  $\lambda_{\text{CuK}\alpha} = 1,54 \text{ \AA}$ ,  $5^\circ \leq 2\theta \leq 60^\circ$ ,  $\Delta 2\theta = 0,02$ , scan rate 2°/min, voltage of 30 kV, current of 15 mA.

Nanoindentations were performed with the aid of Universal Nanomechanical Tester (UNMT) equipped with atomic force microscopy (AFM), produced by Bruker Surface Analysis, USA. Diamond nanoindenter-type Berkovich with tip radius of 70 nm was applied for indentation testing in constant force control mode of 100 mN.

Nanoscratch measurements were made on Hysitron TI 980 instrument (Bruker, MN, USA) by using 2D transducer assembly (both normal and lateral force) equipped with Berkovich probe. A typical radius of curvature for a standard Berkovich probe would be approximately 150 nm. All experiments were conducted at constant load scratch function by applying peak force of 1000  $\mu\text{N}$ .

The morphology of the PLA-based nanocomposites was observed by a scanning electron microscope (FEI Quanta 200 FEG, Hillsboro, OR, USA). 3D-printed samples were immersed in liquid nitrogen, then cut to get visibility of the inner layers in cross-section surface and finally coated with Au/Pd

**Table 1 List of composites tested by nanoindentation technique**

No.	Sample index	PLA content, wt.%	MWCNT content, wt.%	GNP content, wt.%
1	PLA	100	...	...
2	3MWCNT	97	3	...
3	6MWCNT	94	6	...
4	9MWCNT	91	9	...
5	12MWCNT	88	12	...
6	3GNP	97	...	3
7	6GNP	94	...	6
8	9GNP	91	...	9
9	12GNP	88	...	12
10	1.5GNP1.5MWCNT	97	1.5	1.5
11	1.5GNP4.5MWCNT	94	4.5	1.5
12	3GNP3MWCNT	94	3	3
13	4.5GNP1.5MWCNT	94	1.5	4.5
14	3GNP6MWCNT	91	6	3
15	6GNP3MWCNT	91	3	6
16	3GNP9MWCNT	88	9	3
17	9GNP3MWCNT	88	3	9
18	6GNP6MWCNT	88	6	6
19	Black Magic	Unknown	Unknown	Unknown

alloy using an E5 150 SEM coating unit (Polaron Equipment Ltd., Doylestown, PA, USA).

### 3. Results and Discussion

#### 3.1 Structure Analysis of Carbon Nanofillers

Raman analysis has become a useful and proper method in the characterization of carbon nanomaterials molecular morphology. In Fig. 1, there are well-expressed D, G and 2D Raman bands detected in the spectrum of GNPs. The relative high intensity of the Raman G mode of graphene at  $1585\text{ cm}^{-1}$  suggests a carbon hexagonal crystal structure composed of mainly  $sp^2$  bonded carbon in planar sheets. It can be seen low intensity of Raman D band against the G band intensity ( $I_D/I_G = 0.18$ ) indicating the presence of low degree of disorder in the graphene architecture (Ref 19, 20). The regular symmetric shape of 2D Raman band at  $2708\text{ cm}^{-1}$  confirms the good quality of GNPs possessing multilayer graphene structure which is implied from the relatively lower intensity of 2D band against the intensity of the G band ( $I_{2D}/I_G = 0.38$ ).

Much higher intensity ratio of the D band against the G band ( $I_D/I_G = 1.25$ ) and appearance of  $D'$  band at  $1625\text{ cm}^{-1}$  are observed as regards the Raman spectrum of the MWCNTs. It means a lot of disorder in the nanotube structure related to the presence of carbon with  $sp^3$  hybridization, more edges and defects on the outer lattice walls and higher number of layers to the walls of the MWCNTs (Ref 21, 22). Downshift up to  $10\text{ cm}^{-1}$  in D, G and 2D Raman modes of MWCNTs resonances compared to the corresponding bands position in GNPs spectrum is attributed to carbon nanotubes lattice strain effects (Ref 23). The sharpness of the graphene G band infers that the  $sp^2$ -hybridized carbon bonds are for the most part very uniform in nature. Contrariwise the MWCNTs spectrum is littered with numerous bands. This is due to a reduction in molecular symmetry which results in more active Raman scatters. The intensive Raman lines appearing at  $\sim 1104$  and  $\sim 1461\text{ cm}^{-1}$

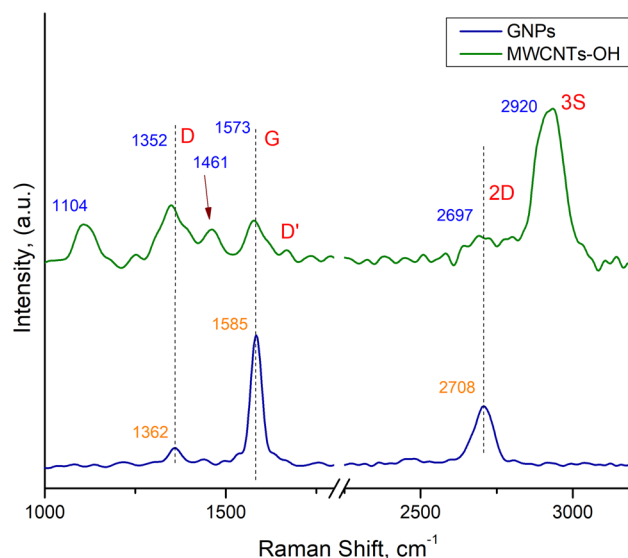


**Fig. 1** Raman spectra comparison of GNPs and -OH-functionalized MWCNTs

can be, respectively, assigned to C-C and C=C stretching vibration modes of amorphous carbon (Ref 24), whereas the prominent 3S band at  $2920\text{ cm}^{-1}$  is associated with graphitization of the nanomaterial (Ref 25).

Partially amorphous carbon structure of the MWCNTs compared to the pristine GNPs can be seen in the XRD patterns of carbon nanofillers, see Fig. 2. A sharp main diffraction (002) peak of graphene nanoplatelets at  $2\theta = 26.3^\circ$  confirms the high degree of crystallinity in the carbon structure. Due to the functionalization, the reflection (002) peak of carbon nanotubes is shifted to  $2\theta = 25.6^\circ$  corresponding to the increase in the interplanar graphitic d spacing from 0.34 to 0.35 nm based on Bragg's law. The same shifting to lower diffraction angle is observed as regards the weak broad XRD peak at  $2\theta = 42.8^\circ$  assigned to graphitic (100) crystalline lattice. X-ray diffraction

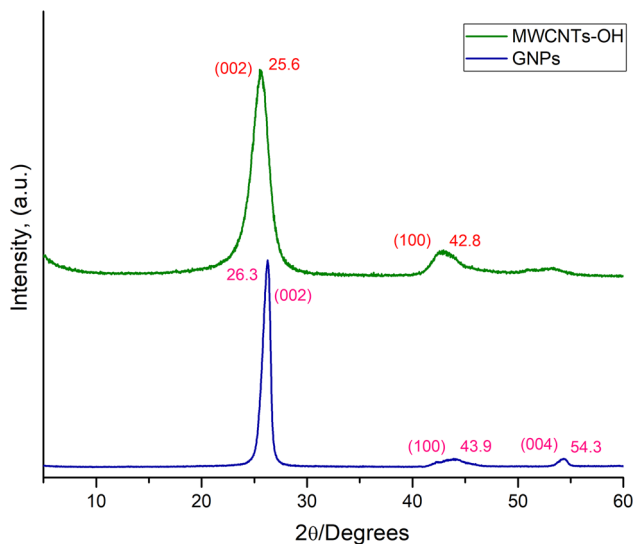


**Fig. 2** XRD patterns of pristine graphene (GNPs) and -OH-functionalized carbon nanotubes (MWCNTs)

pattern at  $2\theta = 54.3^\circ$  is detected in the graphene spectrum indicating (004) carbon crystal lattice.

### 3.2 Nanoindentation Analysis

Nanoindentation hardness and Young's modulus of elasticity were calculated from the drawn load–displacement curves using the method of Oliver and Pharr (Ref 26). These main parameters were received by indentation load and displacement measurements without need to image the hardness impression. Load was measured as a function of penetration depth. A standard test was repeated 48 times ( $4 \times 12$ ; spacing between indents  $80 \mu\text{m}$ ) to have statistical data. There was no need of additional smoothing of the surface since each printed object clung well enough to the printer bed and thus acquired a sufficient flat surface. A depiction of typical indentation experiment was made in our former paper (Ref 27). A holding step is included in the test script because of the influence of the creep on the unloading characteristics since the unloading curve is used to estimate the elastic modulus of the material. Nanoindentation tests were made at maximum loading of 100 mN and retention time of 10 s in order to remove the viscoelastic contribution and to approve the Oliver and Pharr model (Ref 28). The results received during the study are based on that model and the synergistic effect of the carbon nanofillers was suggested from the relevant load–displacement curves (Fig. 3a and b). Following the contact geometry of the unloading process, see the inset in Fig. 3b, the contact depth between the indenter and the composite surface,  $h_c = h_{\text{max}} - h_s$ , can be presented as:

$$h_c = h_{\text{max}} + \varepsilon \frac{P_{\text{max}}}{S} \quad (\text{Eq 1})$$

where  $\varepsilon$  is a constant depending on the indenter geometry (equal to 0.75 for Berkovich indenter),  $P_{\text{max}}$  is the maximum load at maximum displacement  $h_{\text{max}}$ , and  $S$  is the elastic unloading stiffness.

The lower penetration depth  $h_{\text{max}}$  registered for the bifiller nanocomposites against the monofiller samples is plain when

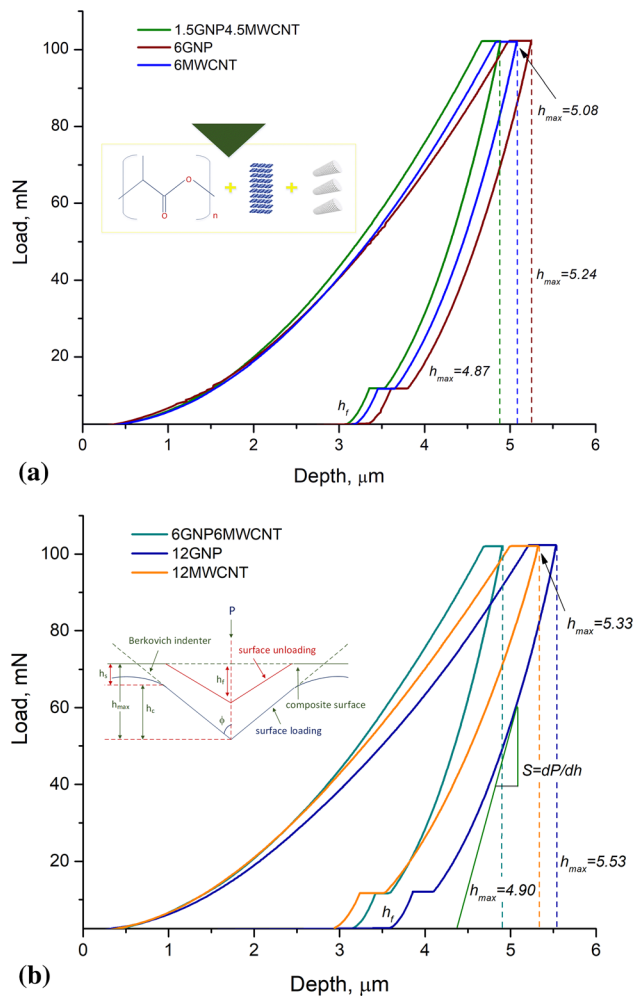


**Fig. 3** Representative load–displacement sensing nanoindentation curves of overall 6 wt.% (a) and 12 wt.% (b) composite loading with rendering a penetration depth dependence on carbon content. Insets: graphic art of the experiment (a) and scheme of the contact geometry throughout nanoindentation testing (b)

analyzing the samples with 6 and 12 wt.% carbon loading, as shown in Fig. 3. That is a fact underlining the presence of synergistic effect of the carbon nanoparticles on the nanocomposite mechanical properties. As the mechanical properties of the PLA are rate sensitive, the effect of different indentation parameters such as loading and unloading times, and retention time at maximum load on the nanocomposite mechanical properties was assessed and compared with available literature data (Ref 29, 30) as well as by means of preliminary tests. According to Oliver&Pharr method, the nanoindentation hardness as a function of indenter's maximum displacement can be estimated from:

$$H = \frac{P_{\text{max}}}{A} \quad (\text{Eq 2})$$

where  $P_{\text{max}}$  is the maximum load at maximum displacement  $h_{\text{max}}$  and  $A$  is the contact area under load between the indenter and the sample surface. Young's modulus ( $E$ ) of the nanocomposite samples is calculated from the effective or reduced elastic modulus ( $E_r$ ) through the relation:



$$E = (1 - \nu^2) \left( \frac{1}{E_r} - \frac{1 - \nu_i^2}{E_i} \right)^{-1} \quad (\text{Eq 3})$$

The reduced elastic modulus considers the fact that elastic displacements befall in both the specimen, with Young's modulus  $E$  and Poisson's ratio  $\nu$ , and the Berkovich indenter with elastic parameters  $E_i$  and  $\nu_i$  (Ref 28). Poisson's ratio of polylactic acid is laid down to be 0.36.

The received data for hardness and Young's modulus as result of nanoindentation tests over GNP/MWCNT/PLA nanocomposites with overall 3 and 6 wt.% carbon loading are presented in Fig. 4(a) and (b). There can be noticed high hardness and elasticity of nearly all 3D-printed nanocomposite samples, most visibly concerning the mixed compound 1.5 wt.% GNP/4.5 wt.% MWCNT/PLA along with registering of excellent and highest Young's modulus of the nanocomposite 3 wt.% GNP/3 wt.% MWCNT/PLA (4.392 GPa). Using two geometrically diverse carbon fillers, such as GNPs and MWCNTs, could induce the formation of compact and sustainable network in the polymer, and thus, to obtain nanocomposites with better mechanical properties. A determinant factor defining these properties is the ratio between the nanofillers in the PLA matrix. The synergistic effect is considerably expressed in better mechanical performance for the bifiller compounds against the monofiller compounds. Comprehending that notion, it has to be mentioned one single exception—22% higher nanomechanical hardness of the com-

posite 6 wt.% MWCNT/PLA compared to pure PLA. This result can be anticipated as an outcome of the remarkable stiffness of pure carbon nanotubes homogeneously dispersed in composite matrix (Ref 31). Serious improvement of elastic modulus and nanoindentation hardness has been reported for PLA-based composite modified with graphene nanoscrolls as nucleating agent (Ref 32). The positive effect is explained with superior level of interfacial interactions and strain in this particular type of carbon nanofiller resulting in better load transfer between graphene nanoparticles and polymer matrix. However, the nanoscrolls dimensionality, the lower PLA grade, and the extremely small indentation load and indentation depth have to be kept in mind.

Investigation of the nanomechanical properties of some selected monofiller and bifiller composite specimens wielding 6 wt.% GNPs and/or MWCNTs but made by different preparation techniques is summarized in Table 2. The level of nanocomposite performance was compared to the values obtained from nanoindentation of the commercial carbon-based material Black Magic. The results indicated the effect of sample pretreatment on nanoindentation analysis that appeared to be much more precise made on flat 3D-printed surface likened to hot pressed material or diamond cut filament and therefore resulting in lower standard deviations of the main estimated parameters—nanohardness and Young's modulus. Black Magic taken as benchmark exhibited lower nanomechanical properties and significant scattering of the values compared to the composite 1.5 wt.% GNP/4.5 wt.% MWCNT/PLA even considering the supplemental fusion of the filament during 3D printing as a factor having impact on material crystalline structure. High standard error of the results received from nanoindentation of diamond cut Black Magic filament against the 3D-printed plates is a confirmation of the advantage of 3D printing as sample preparation method. Recent nanoindentation study on 3D-printed specimens of neat PLA and Black Magic has been made at 14 mN peak load and 1.3-2.2  $\mu\text{m}$  range of penetration depths (Ref 30). The reported nanomechanical characteristics of Black Magic correspond to the values of the 3D-printed bifiller composite samples possessing best nanoindentation hardness and Young's modulus illustrated in Figs. 4 and 5.

Excellent characteristics in terms of hardness (243 MPa) and elasticity (4.467 GPa) of the nanocomposite 6 wt.% GNP/6 wt.% MWCNT/PLA can be perceived in the plotted column graphs shown in Fig. 5, including an appearance of noticeably high Young's modulus belonging to the compound 6 wt.% GNP/3 wt.% MWCNT/PLA (4.437 GPa). Once again it was detected better mechanical performance looking the values of the bifiller composites 9 wt.% GNP/3 wt.% MWCNT/PLA and 3 wt.% GNP/9 wt.% MWCNT/PLA compared to the monofiller composites 12 wt.% GNP/PLA and 12 wt.% MWCNT/PLA. Regarding the monofiller nanocomposites, it should be noted a significant nanoindentation hardness of the compound 9 wt.% MWCNT/PLA possibly related to good filler dispersion. Nanosized nucleating carbon nanoparticles are known to reinforce the mechanical properties of polymer matrices by increment of the interactions between the polymer chains and the carbon filler owning high surface area (Ref 33). The low Young's modulus of the composite 12 wt.% GNP/PLA might be due to formation of aggregates and fractional inhomogeneous distribution of graphene nanoplatelets in the polymer matrix. A similar nonuniform nanofiller insertion can be the reason for relatively poor nanomechanical properties of the

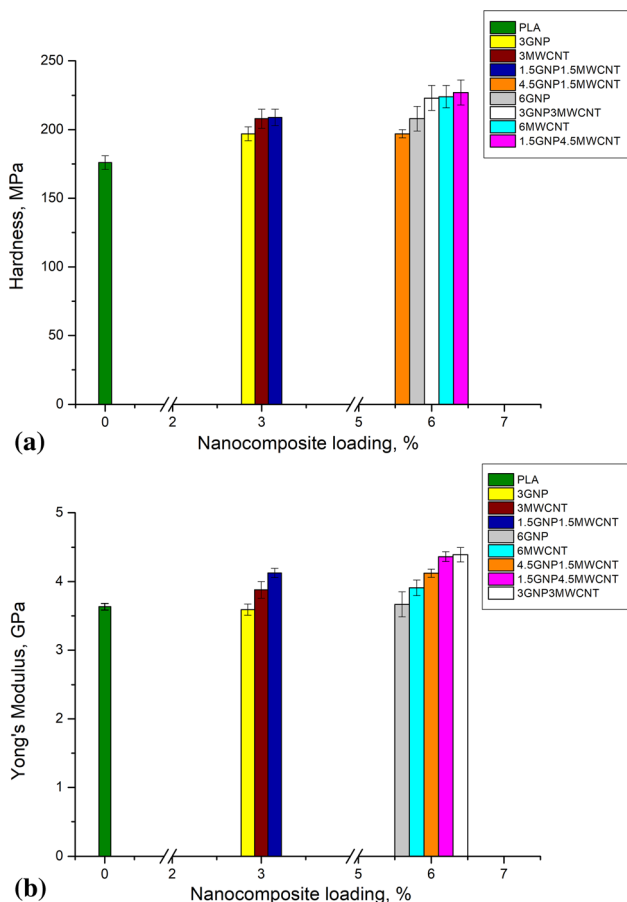


**Fig. 4** Hardness (a) and Young's modulus (b) of GNP/MWCNT/PLA nanocomposites with overall 3 and 6 wt.% carbon loading

**Table 2 Hardness and Young's modulus data defined by nanoindentation tests on diverse composite samples including Black Magic as a benchmark**

No.	Sample	Preparation	Hardness, MPa	Elasticity, GPa
1	4.5wt.%GNP1.5wt.%MWCNT/PLA	3D-printed plate	197 ± 3	4.123 ± 0.060
2	1.5wt.%GNP4.5wt.%MWCNT/PLA	3D-printed plate	227 ± 9	4.967 ± 0.071
3	4.5wt.%GNP1.5wt.%MWCNT/PLA	Diamond cut filament	216 ± 16	4.725 ± 0.198
4	1.5wt.%GNP4.5wt.%MWCNT/PLA	Diamond cut filament	201 ± 5	3.371 ± 0.723
5	6wt.%GNP/PLA	Hot pressed thin film	206 ± 18	4.025 ± 0.225
6	6wt.%MWCNT/PLA	Hot pressed thin film	204 ± 14	3.352 ± 0.147
7	Black Magic	Diamond cut filament	222 ± 35	3.948 ± 0.469
8	Black Magic	Hot pressed thin film	190 ± 16	3.522 ± 0.246

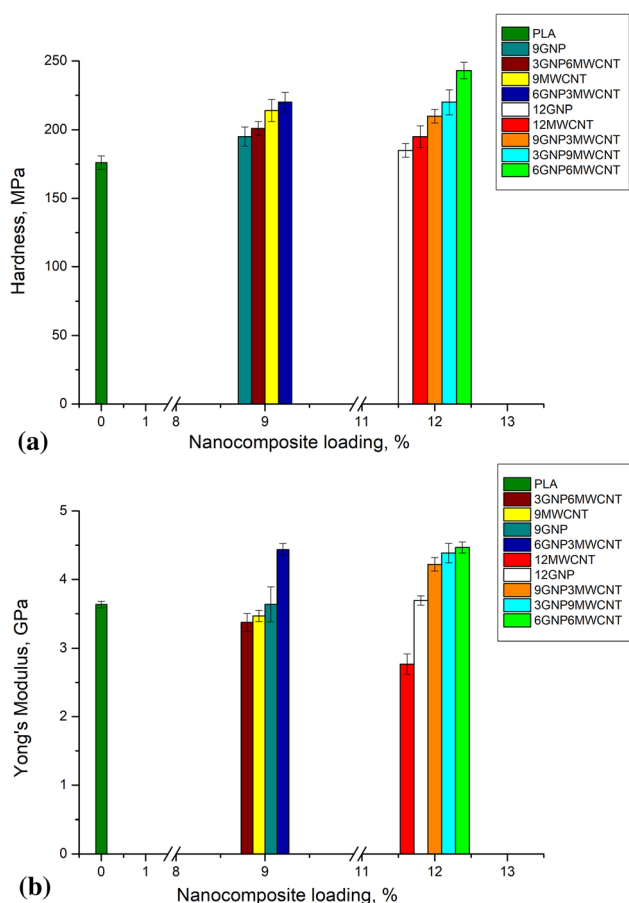


**Fig. 5** Hardness (a) and Young's modulus (b) of GNP/MWCNT/PLA nanocomposites with overall 9 and 12 wt.% carbon loading

compound 3 wt.% GNP/6 wt.% MWCNT/PLA, see Fig. 5. However, the hardness value of the latter is higher than the hardness calculated through nanoindentation testing of the monofiller composite 9 wt.% GNP/PLA.

### 3.3 Nanoscratch Analysis

An advanced nanoscratch testing was conducted over two bifiller composite samples holding 6 and 12 wt.% content of carbon nanofillers whereafter the results were contrasted to the scratch resistance data of monofiller composite samples having the same total weight percent content of GNPs or MWCNTs (Fig. 6).

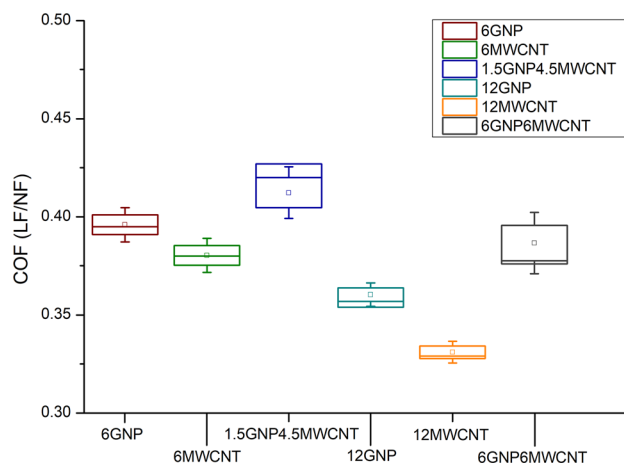


**Fig. 6** COF data from nanoscratch testing of two bifiller and four monofiller composite specimens using three-side pyramidal Berkovich probe

The fulfillment of scratch data analysis is based on normal force, normal displacement, lateral force, and lateral displacement parameters which are all usually drawn as function of time. Constant load scratch function consists of several segments, but extraction of the coefficient of friction (COF) was made from the graph conforming to the only segment of interest which is actually the segment that performs the nanoscratch. COF is calculated by the ratio of the exerted lateral force during material plowing to the constant normal force set in load function. Apparently the friction coefficient depends on nanocomposites properties as material hardness and the COF value could measure the surface resistance of a composite against scratch (Ref 34). Motion of Berkovich indenter over harder specimen surface will bring to raised lateral force that would mean higher material resistance to scratch. Representation of COF data glancing the variation of lateral force as regards the applied normal force and therefore fixing the nanocomposite scratch resistance can be found in the plotted box chart, see Fig. 6. Synergy of combining GNPs and MWCNTs as two carbon nanofillers incorporated in PLA matrix is displayed again, this time pointing out higher scratch resistance of the bifiller composites compared to monofiller composites with same carbon loading. Different surface strain behavior of the nanocomposites is inferred by the variation of the ascertained COF values. The reliability of nanoscratch study requires flat enough sample surface in order to perform successful experiments with low peak force of 1000  $\mu\text{N}$ . In situ

**Table 3 Average surface roughness and residual track depth received by in situ SPM imaging of nanoscratch tests on monofiller and bifiller composite samples**

No	Nanocomposite	Average roughness, nm	Residual depth, nm
1	6wt.%GNP/PLA	5.6	195.3
2	6wt.%MWCNT/PLA	11.3	144.9
3	1.5wt.%GNP4.5wt.%MWCNT/PLA	4.1	124.1
4	12wt.%GNP/PLA	7.3	141.3
5	12wt.%MWCNT/PLA	9.3	134.3
6	6wt.%GNP6wt.%MWCNT/PLA	10.7	98.0

scanning probe microscopy (SPM) imaging of specimens' scratch surface area showed that the average roughness (Ra) of the composite samples is in the range 4-11 nm, see Table 3. These values validate the 3D printing as one excellent method of elaborating test samples, fit for both nanoindentation and nanoscratch analyses. Astounding topography forward and 3D in situ SPM images are presented in Fig. 7(a) and (b).

The marker depicted in Fig. 7(a) was used to estimate the vertical distance into a scratch trace as consequence of indenter displacement (Table 3). Clear idea about formation of material pile-up along the scratch groove, track residual depth after load removal and view of composite surface roughness are engrossed by the 3D image in Fig. 7(b). The observed folds within the scratch track are indication for repeating increment and release of lateral force during the test as a result of the viscoelastic nature of polymer matrix (Ref 35). Interestingly, the pile-up of material is concentrated on the right side of the groove that could be due to the onset angle of indenter move and to composite surface strength resisting the probe motion through the sample. The residual scratch depth shifted upward by blending GNPs and MWCNTs in the composite structure, disclosing that bifiller nanocomposites are harder and higher tangential force has to be applied to perform nanoscratch.

### 3.4 Scanning Electron Microscopy Analysis

SEM microscopy is widely reported as physical method for morphological characterization of carbon fillers inserted in polymer-based nanocomposites (Ref 36, 37). GNPs and MWCNTs have strong impact on the entire composite microstructure revealed by the SEM images. Nanocomposite materials can be reckoned for hybrid materials only when the carbon nanoparticles are homogenously dispersed in a polymer die (Ref 38). Another important factor is the dimensionality of carbon nanofillers primarily influencing on the supramolecular structure of PLA-based nanocomposite (Ref 39). The micrographs presented in Fig. 8 were made by focusing the instrument over cross-section sample surface. The received SEM images of bifiller nanocomposites 3 wt.% GNP/3 wt.% MWCNT/PLA (Fig. 8a), 1.5 wt.% GNP/4.5 wt.% MWCNT/PLA (Fig. 8b), 3 wt.% GNP/9 wt.% MWCNT/PLA (Fig. 8c) and 6 wt.% GNP /6 wt.% MWCNT/PLA (Fig. 8d) revealed good uniform distribution of carbon nanoparticles in shape of stacked graphene sheets and peaking worm-like nanotubes located within the PLA matrix. These findings are in full agreement with the established nanomechanical characteristics of the above-mentioned samples being the highest among the whole series modified with 6 wt.% and 12 wt.% content of carbon nanofillers. The appearance of few cracks is an indication of embrittlement in the composites. These cracks

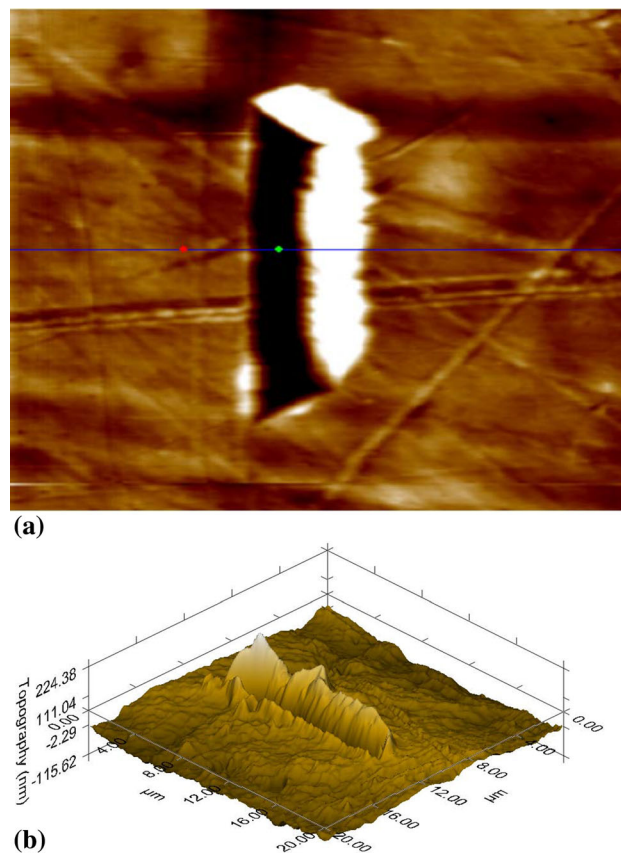


**Fig. 7** In situ SPM topography forward (a) and 3D (b) images of nanoscratch test made on the surface of 1.5 wt.% GNP/4.5 wt.% MWCNT/PLA composite sample

are most probably due to the samples breaking in order to prepare them for SEM analysis. It can be inferred that the combination of two allotropic types of carbon nanoparticles forms an interconnected network in the polymer matrix that leads to unique synergistic effect in the refinement of the composite mechanical properties demonstrated by nanoindentation testing.

## 4. Conclusions

Nanoindentation and nanoscratch as nanomechanical characterization techniques were met to uphold the synergistic effect of graphene and carbon nanotubes on the mechanical properties of PLA-based nanocomposites. Good carbon



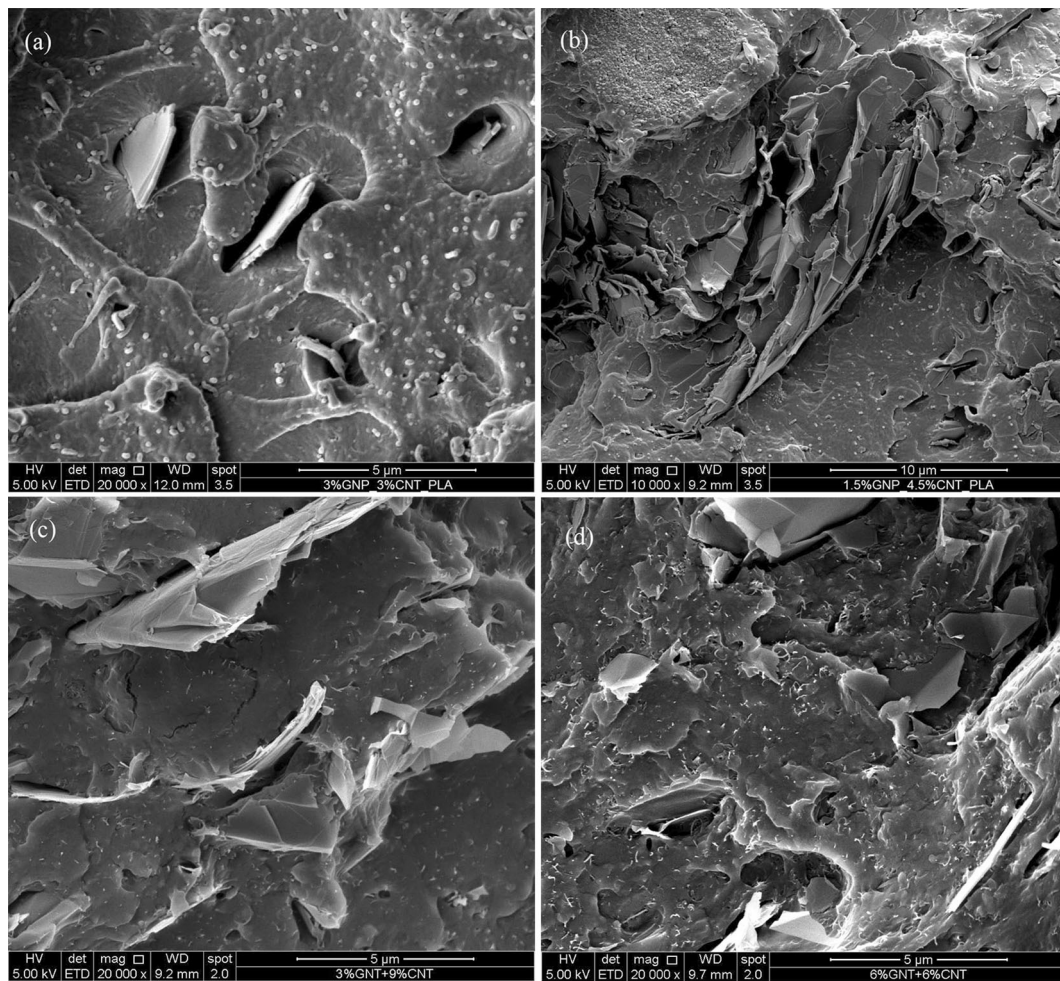


**Fig. 8** SEM micrographs of nanocomposite specimens 3 wt.% GNP/3 wt.% MWCNT/PLA (a), 1.5 wt.% GNP/4.5 wt.% MWCNT/PLA (b), 3 wt.% GNP/9 wt.% MWCNT/PLA (c) and 6 wt.% GNP/6 wt.% MWCNT/PLA (d)

nanoparticles distribution in the polymer matrix, suggested as outcome of implemented nanomechanical testing, was confirmed by SEM analysis of the composites having mixed GNPs and MWCNTs loading. Generally, the graphene filler improved the elastic properties of nanocomposites, whereas the carbon nanotubes were found to be responsible for better nanohardness of the compounds. The synergism of two forms of carbon nanomaterials was affirmed by definition of the nanomechanical surface characteristics of the bifiller composite materials. This mechanical reinforcement of the nanocomposites is probably related to the specific structure and geometry of the hybrid nanofillers, the interactions in GNPs and MWCNTs, the stress transfer along the interface nanofiller-polymer, and the impact of melt mixing preparation method. It should be emphasized that the synergistic effect as regards nanoindentation data is more pronounced for higher carbon concentrations in the PLA matrix, for instance at overall 9 and 12 wt.% carbon content in the bifiller composites. The average surface roughness and residual depth are key parameters that one can use to ascertain the mechanism entangled in the nanoscratch behavior of composite materials. Greater reduction of the vertical distance in residual scratch grooves was detected for nanocomposite samples containing both GNPs and MWCNTs. According to melt extrusion process and evidenced by SEM

micrographs, the graphene nanoplatelets and the carbon nanotubes seem to be highly dispersed in the composite die.

### Acknowledgments

This work has received funding by the European Union's Horizon 2020-MSCA-RISE-734164 Graphene 3D Project and by the H2020-FET-Graphene Flagship-881603 Graphene Core 3 Project. The authors from Institute of Mechanics would like to acknowledge the contribution of the Bilateral collaboration between IMech, BAS and IPCB-CNR, Napoli/Portici (2019-2021). This study has also been accomplished with the financial support by the Grant No BG05M2OP001-1.002-0011, financed by the Science and Education for Smart Growth Operational Program (2014-2020) and co-financed by the European Union through the European structural and Investment funds.

### References

1. R. Kotsilkova, E. Ivanov, E. Krusteva, S. Silvestre, S. Cimmino and D. Duraccio, *Ecosustainable Polymer Nanomaterials for Food Packaging*, 1st ed. CRC Press, Boca Raton, 2013, p 55–86. (Chap. 3)



2. E. Stoleru, Y. Tsekov, R. Kotsilkova, E. Ivanov and C. Vasile, Mechanical Behavior at Nanoscale of Chitosan-Coated PE Surface, *J. Appl. Polym. Sci.*, 2015, **132**, p 42344
3. J. Kwon, M.C. Brandes, P.S. Phani, A.P. Pilchak, Y.F. Gao, E.P. George, G.M. Pharr and M.J. Mills, Characterization of Deformation Anisotropies in an  $\alpha$ -Ti Alloy by Nanoindentation and Electron Microscopy, *Acta Mater.*, 2013, **61**, p 4743–4756
4. J.L. Wu, Y. Pan and J.H. Pi, Evaluation of Cu-Zr-Ti-In Bulk Metallic Glasses via Nanoindentation, *J. Mater. Eng. Perform.*, 2013, **22**, p 2288–2292
5. D. Catoor, Y.F. Gao, J. Geng, M.J.N.V. Prasad, E.G. Herbert, K.S. Kumar, G.M. Pharr and E.P. George, Incipient Plasticity and Deformation Mechanisms in Single-Crystal Mg During Spherical Nanoindentation, *Acta Mater.*, 2013, **61**, p 2953–2965
6. J. Němeček, *Nanoindentation in Materials Science*, 1st ed. IntechOpen, London, 2012, p 89–108. (Chap. 4)
7. A.M. Diez-Pascual, M.A. Gómez-Fatou, F. Ania and A. Flores, Nanoindentation in Polymer Nanocomposites, *Prog. Mater. Sci.*, 2015, **67**, p 1–94
8. A.C. Fischer-Cripps, *Nanoindentation*, 2nd ed. Springer, New York, 2004, p 1–212
9. M. Moniruzzaman and K.I. Winey, Polymer Nanocomposites Containing Carbon Nanotubes, *Macromolecules*, 2006, **39**, p 5194
10. B. Fiedler, F. Gojny, M.H.G. Wichmann, M.C.M. Nolte and K. Schulte, Fundamental Aspects of Nano-reinforced Composites, *Compos. Sci. Technol.*, 2006, **66**, p 3115
11. F. Hussain, M. Hojjati, M. Okamoto and R.E. Gorga, Review article: Polymer-Matrix Nanocomposites, Processing, Manufacturing, and Application: An Overview, *J. Compos. Mater.*, 2006, **40**, p 1511
12. M. Cadek, J.N. Coleman, V. Barron, K. Hedrick and W.J. Blau, Morphological and Mechanical Properties of Carbon-Nanotube-Reinforced Semicrystalline and Amorphous Polymer Composites, *Appl. Phys. Lett.*, 2002, **81**, p 1523
13. H.C. Schniepp, J.L. Li, M.J. McAllister, H. Sai, M. Herrera-Alonso, D.H. Adamson, R.K. Prud'homme, R. Car, D.A. Saville and I.A. Aksay, Functionalized Single Graphene Sheets Derived from Splitting Graphite Oxide, *J. Phys. Chem. B*, 2006, **110**, p 8535
14. B. Das, K.E. Prasad, U. Ramamurty and C.N.R. Rao, Nano-indentation Studies on Polymer Matrix Composites Reinforced by Few-Layer Graphene, *Nanotechnology*, 2009, **20**, p 125705
15. K.E. Prasad, B. Das, U. Maitra, U. Ramamurty and C.N.R. Rao, Extraordinary Synergy in the Mechanical Properties of Polymer Matrix Composites Reinforced with 2 Nanocarbons, *PNAS*, 2009, **106**, p 13186–13189
16. M.M. Shokrieh, M.R. Hosseinkhani, M.R. Naimi-Jamal and H. Tourani, Nanoindentation and Nanoscratch Investigations on Graphene-Based Nanocomposites, *Polym. Test.*, 2013, **32**, p 45–51
17. B. Hwang, S. Lim, M. Park and S.M. Han, Neutral Plane Control by Using Polymer/Graphene Flake Composites for Flexible Displays, *RSC Adv.*, 2017, **7**, p 8186–8191
18. S. Chatterjee, F. Nafezarefi, N.H. Tai, L. Schlagenhauf, F.A. Nüesch and B.T.T. Chu, Size and Synergy Effects of Nanofiller Hybrids Including Graphene Nanoplatelets and Carbon Nanotubes in Mechanical Properties of Epoxy Composites, *Carbon*, 2012, **50**, p 5380–5386
19. R. Beams, L.G. Cancado and L. Novotny, Raman Characterization of Defects and Dopants in Graphene, *J. Phys. Condens. Matter.*, 2015, **27**, p 83002
20. S. Das, S. Khanna and D.P. Mondal, Graphene-Reinforced Aluminum Hybrid Foam: Response to High Strain Rate Deformation, *J. Mater. Eng. Perform.*, 2019, **28**, p 526–534
21. S. Osswald, M. Havel and Y. Gogotsi, Monitoring Oxidation of Multiwalled Carbon Nanotubes by Raman Spectroscopy, *J. Raman Spectrosc.*, 2007, **38**, p 728–736
22. D. Singh, P.K. Iyer and P.K. Giri, Diameter Dependence of Interwall Separation and Strain in Multiwalled Carbon Nanotubes Probed by X-ray Diffraction and Raman Scattering Studies, *Diam. Relat. Mater.*, 2010, **19**, p 1281–1288
23. R. Kumar and S.B. Cronin, Raman Scattering of Carbon Nanotube Bundles Under Axial Strain and Strain-Induced Debundling, *Phys. Rev. B*, 2007, **75**, p 155421
24. L. Bokobza, J.-L. Bruneel and M. Couzi, Raman Spectroscopic Investigation of Carbon-Based Materials and Their Composites. Comparison Between Carbon Nanotubes and Carbon Black, *Chem. Phys. Lett.*, 2013, **590**, p 153–159
25. P. Fernandes-Ibanez, M.I. Polo-Lopez, S. Malato, S. Wadhwa, J.W.J. Hamilton, P.S.M. Dunlop, R. D'Sa, E. Magee, K. O'Shea, D.D. Dionysiou and J.A. Byrne, Solar Photocatalytic Disinfection of Water Using Titanium Dioxide Graphene Composites, *Chem. Eng. J.*, 2015, **261**, p 36–44
26. W.C. Oliver and G.M. Pharr, An Improved Technique for Determining Hardness and Elastic Modulus Using Load and Displacement Sensing Indentation Experiments, *J. Mater. Res.*, 1992, **7**, p 1564–1583
27. T. Bataklijev, V. Georgiev, E. Ivanov, R. Kotsilkova, R. Di Maio, C. Silvestre and S. Cimmino, Nanoindentation Analysis of 3D Printed Poly(Lactic Acid)-Based Composites Reinforced with Graphene and Multiwall Carbon Nanotubes, *J. Appl. Polym. Sci.*, 2019, **136**(13), p 47260
28. W.C. Oliver and G.M. Pharr, Measurement of Hardness and Elastic Modulus by Instrumented Indentation: Advances in Understanding and Refinements to Methodology, *J. Mater. Res.*, 2004, **19**, p 3–20
29. E.P. Koumoulos, M. Valentin, D.A. Dragatogiannis, C.A. Charitidis, I. Krupa and I. Novak, Nanomechanical Properties of Plasma Treated Polylactic Acid, *Plast. Rubber Compos.*, 2015, **8**, p 322–329
30. M. Mansour, K. Tsongas and D. Tzetzis, Measurement of the Mechanical and Dynamic Properties of 3D Printed Polylactic Acid Reinforced with Graphene, *Polym. Plast. Technol.*, 2019, **58**(11), p 1234–1244
31. C.R. Bradbury, J.-K. Gomon, L. Kollo, H. Kwon and M. Leparoux, Hardness of Multi Wall Carbon Nanotubes Reinforced Aluminium Matrix Composites, *J. Alloys Compd.*, 2014, **585**, p 362–367
32. O. Ajala, C. Werther, P. Nikaen, R.P. Singh and D. Depan, Influence of Graphene Nanoscrolls on the Crystallization Behavior and Nanomechanical Properties of Polylactic Acid, *Polym. Adv. Technol.*, 2019, **30**, p 1825–1835
33. L. Zhang, Y. Li, H. Wang, Y. Qiao, J. Chen and S. Cao, Strong and Ductile Poly(Lactic Acid) Nanocomposite Films Reinforced with Alkylated Graphene Nanosheets, *Chem. Eng. J.*, 2015, **264**, p 538–546
34. E.P. Koumoulos, P. Jagadale, A. Lorenzi, A. Tagliaferro and C.A. Charitidis, Evaluation of Surface Properties of Epoxy-Nanodiamonds Composites, *Compos. Part B*, 2015, **80**, p 27–36
35. A. Dasari, Z.-Z. Yu and Y.-W. Mai, Nanoscratching of Nylon 66-Based Ternary Nanocomposites, *Acta Mater.*, 2007, **55**, p 635–646
36. Y.Z. Keteklahijani, M. Arjmand and U. Sundararaj, Cobalt Catalyst Grown Carbon Nanotube/Poly(Vinylidene Fluoride) Nanocomposites: Effect of Synthesis Temperature on Morphology, Electrical Conductivity and Electromagnetic Interference Shielding, *ChemistrySelect*, 2017, **2**, p 10271–10284
37. N. Vidakis, A. Maniadi, M. Petousis, M. Vamvakaki, G. Kenanakis and E. Koudoumas, Mechanical and Electrical Properties Investigation of 3D-Printed Acrylonitrile-Butadiene-Styrene Graphene and Carbon Nanocomposites, *J. Mater. Eng. Perform.*, 2020, **29**, p 1909–1918
38. U. Szeluga, B. Kumanek and B. Trzebicka, Synergy in Hybrid Polymer/Nanocarbon Composites. A Review, *Compos. Part A*, 2015, **73**, p 204–231
39. H. Bai, W. Zhang, H. Deng, Q. Zhang and Q. Fu, Control of Crystal Morphology in Poly(L-lactide) by Adding Nucleating Agent, *Macromolecules*, 2011, **44**(6), p 1233–1237

**Publisher's Note** Springer Nature remains neutral with regard to jurisdictional claims in published maps and institutional affiliations.